# MAGNETIC AND GALVANOMAGNETIC PROPERTIES OF CdSb DOPED WITH Ni

**E. Lähderanta[1], R. Laiho[2], A.V. Lashkul[1, 2], K.G. Lisunov[3*], M.A. Shakhov[4], and V.S. Zakhvalinskii[5]**

*[1]Department of Physics and Mathematics, Lappeenranta University of Technology, FIN-53851, Lappeenranta, Finland*
*[2]Wihuri Physical Laboratory, University of Turku, FIN-20014, Turku, Finland*
*[3]Institute of Applied Physics, Academy of Sciences of Moldova, 5, Academiei str., MD-2028, Chisinau, Republic of Moldova*
*[4]A. F. Ioffe Physico-Technical Institute, 194021, St. Petersburg, Russia*
*[5]Department of Physics, Belgorod State University, RUS-308015, Belgorod, Russia*
*[*]Corresponding author, e-mail: kgl-is-here@rambler.ru, kgl40@hotmail.com*
(Received 23 September 2008)

## Abstract

Magnetic and galvanomagnetic properties of the group II-V semiconductor CdSb single crystals doped with Ni are reported. The magnetization data give evidence for spheroidal Ni-rich $Ni_{1-x}Sb_x$ nanoclusters. Mechanism of the low-temperature conductivity is sensitive to the magnetic field, being of the variable-range hopping type in zero field and of the nearest-neighbor hopping type in strong fields. The Hall resistivity contains the normal and the anomalous contributions.

## 1. Introduction

Progress in spintronics suggests expansion of its materials base by search of new appropriate magnetic systems. An important role at this point is played by diluted magnetic semiconductors (DMS), including those with nanosize magnetic precipitates [1]. Recently, a family of such materials has been enriched with cadmium antimonide doped with Ni, p-CdSb:Ni [2, 3]. Undoped CdSb is the group II-V orthorhombic semiconductor with strongly anisotropic transport properties [4]. Doping of CdSb with Ni leads to a secondary magnetic phase, which at a small doping level consists of an assembly of magnetic Ni-rich $Ni_{1-x}Sb_x$ nanosize spheroidal clusters [2, 3].

In this work, we review investigations of magnetization of CdSb:Ni giving evidence for $Ni_{1-x}Sb_x$ nanoclusters [2, 3]. Also, new measurements of galvanomagnetic properties of p-CdSb:Ni, including the hopping conductivity, the magnetoresistance (MR), and the Hall effect are presented and analyzed taking into account contribution due to magnetic $Ni_{1-x}Sb_x$ nanoparticles.

## 2. Results and discussion

Single crystals of p-CdSb doped with 2 at % of Ni were prepared by a modified Bridgman method [4]. Measurements of the dc magnetization, $M$, were performed in a field, $B$, parallel to one of the crystallographic axes [100], [010], and [001] after cooling the sample in zero field (ZFC) or in a field (FC). Measurements of the resistivity and MR were made in zero magnetic field, $B$, or in pulsed fields up to $B$ = 30 T, in transversal configurations with **j** || [100] and **B** || [001] (# 1), **j** || [010] and **B** || [100] (# 2), **j** || [001] and **B** || [010] (# 3).

### 2.1. Magnetic properties

A clear irreversibility of the low-field magnetic susceptibility, $\chi$, is evident from Fig. 1 (a) below 300 K, including the deviation of the plots of $\chi_{ZFC}$ ($T$), $\chi_{FC}$ ($T$) and broad maximum of $\chi_{ZFC}$ ($T$) at $T_b \sim 100$ K. Evolution of these properties with increasing $B$ displays a tendency towards collapsing of both branches of $\chi$ ($T$) into a single curve above ~ 4 kG and decrease of $T_b$. The important features of the behavior of magnetization in strong fields following from Fig. 1 (b) (the scattering of the data points is connected to subtraction of the diamagnetic contribution) are the rapid saturation of the plots of $M$ ($B$) with increasing $B$, the weak dependence of the saturated magnetization, $M_s$, on $T$ and the large anisotropy of $M_s$ evident from the inset to Fig. 1 (b). The hysteresis of the $M$ ($B$) curves is observed already at 300 K, whereas the coercivity, $B_c$ ($T$), exhibits anisotropy, which is inverted with respect to that of $M_s$ ($T$) (see Fig. 2 (a)).

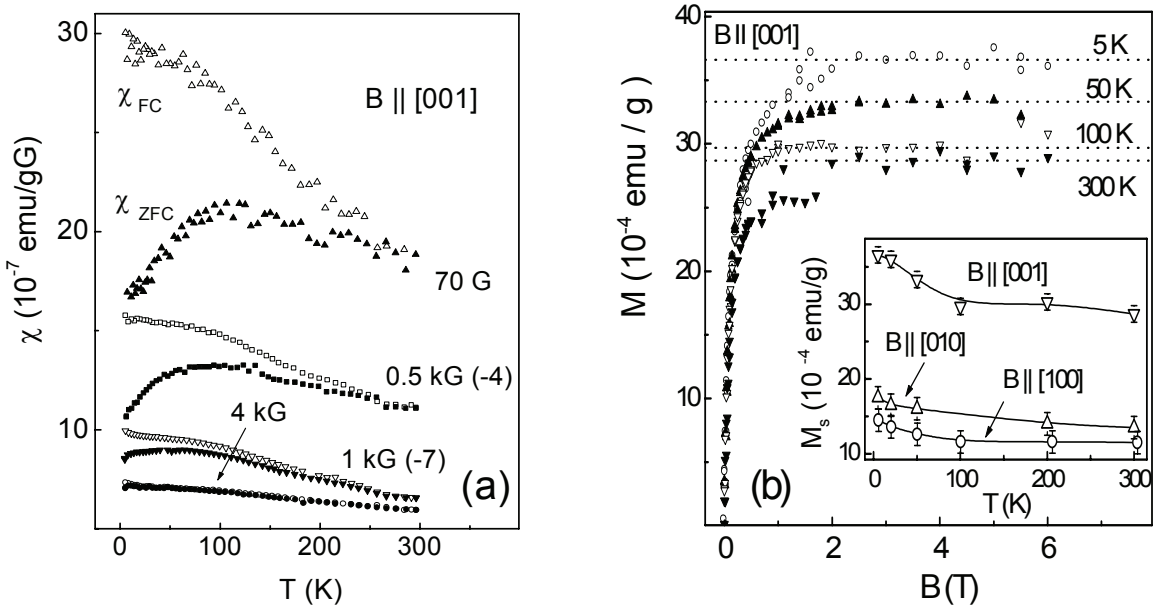


Fig. 1. Plots of $\chi_{FC}$ (open symbols) and $\chi_{ZFC}$ (closed symbols) vs. $T$ (a) and $M$ vs. $B$ (b). Inset: $M_s$ vs. $T$. Some curves in the (a) panel are shifted along the Y- axes by the values shown in parenthesis.

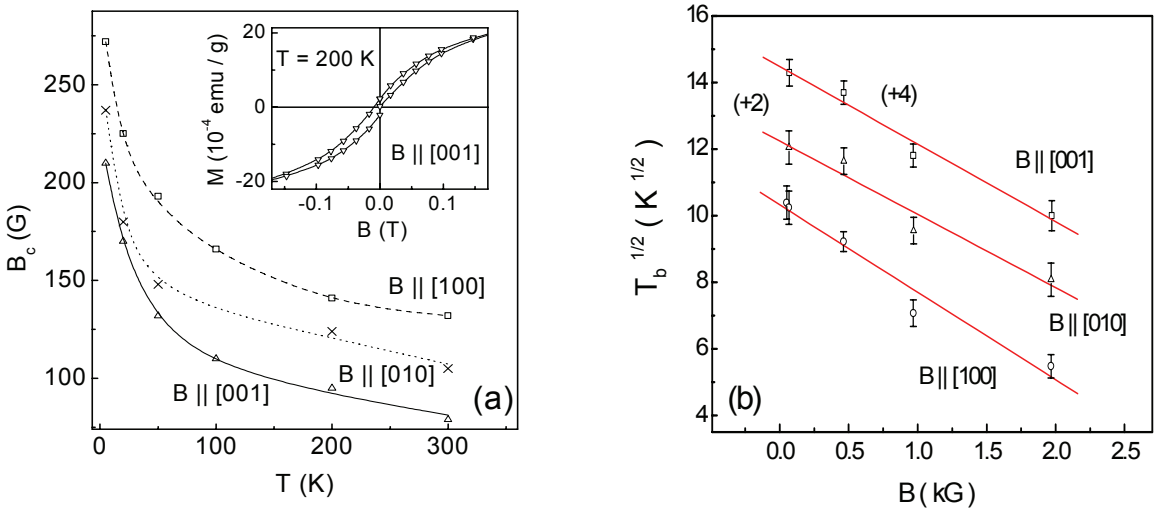


Fig. 2. Hysteresis curve (inset), dependence of coercivity on $T$ (a) and plots of $T_b^{1/2}$ vs. $B$ (b).

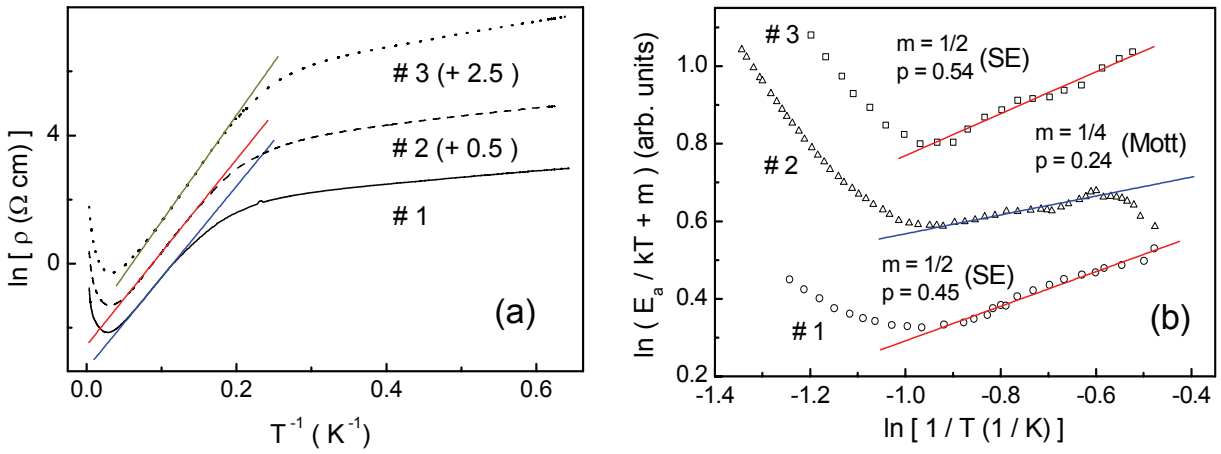


Fig. 3. Plots of ln ρ vs. $T^{-1}$ (a) and of ln ($E_a$ / $kT$ + m) vs. ln (1 / $T$) (b) at $B$ = 0.

The low-field irreversibility in Fig. 1 (a), as well as the rapid saturation of $M$ ($B$), and weak temperature dependence of $M_s$ in Fig. 1 (b) are typical of an assembly of magnetic nanoclusters or nanosize Ni-rich $Ni_{1-x}Sb_x$ inclusions. Namely, blocking of the moments of the $Ni_{1-x}Sb_x$ clusters due to the anisotropy energy barriers, affected by the external field, leads to deviations of $\chi_{ZFC}$ ($T$) and $\chi_{FC}$ ($T$) until $B$ is smaller than the mean anisotropy field, $B_K$. In turn, reduction of the barriers by $B$ is responsible for the magnetic-field dependence of $T_b$ yielding the following relations: $T_b$ ($B$) / $T_b$ (0)]$^{1/2}$ ≈ 1 – $B$ / $B_K$ and $B_K$ / $T_b$ (0) ≈ 50 $k_B$ /μ, where μ is the mean cluster moment [5]. As follows from Fig. 2 (b), the function $T_b$ ($B$) is close to the first of these relations, giving $T_b$ (0) = 105 ± 5 K and $B_K$ = 4.4 ± 0.5 kG, whereas with the second relation we obtain μ = (1.8 ± 0.2)×10$^4$ $\mu_B$. One can also see that $B_K$ obtained from the analysis in Fig. 2 (b) is the same as the field (~ 4 kG) in which the low-field magnetic irreversibility in Fig. 1 (a) vanishes. Finally at this point, the magnetic-field and temperature dependences of the magnetization in Fig. 1 (b) are in general agreement with the corresponding behavior of the ferromagnetic $Ni_{1-x}Sb_x$ secondary phase, having only a minor part of Ni ions, whereas the majority on Ni in our p-CdSb:Ni samples forms a paramagnetic subsystem.

As mentioned above, undoped CdSb is the anisotropic material. Therefore, probably the most important feature of CdSb:Ni attracting interest to this compound and its possible applications as the DMS, is the anisotropy of the magnetic properties as shown in the inset to Fig. 1 (b) and in Fig. 2 (a). A detailed analysis has demonstrated that this feature is due to large nonsphericity (or high aspect ratio of $m = l/r$, where $l$ is the longitudinal size and $r$ is the radius) of the $Ni_{1-x}Sb_x$ nanoclusters, accompanied by their single-domain structure, broad size distribution, and preferred orientation of the major axis. The values of $m$ ~ 4 – 8 and $r$ ~ 2.6 – 3.6 nm, as well as the volume fraction of the $Ni_{1-x}Sb_x$ phase η' ~ (0.6 – 0.9)× 10$^{-4}$, have been estimated [2, 3].

## 2.2. Resistivity and magnetoresistance

As can be seen from Fig. 3 (a), the resistivity, ρ, at $B$ = 0 has two intervals of the activated behavior, characterized by different slopes. The high-temperature slope is due to activation of holes from the acceptor band (AB) into the valence band (VB). The low-temperature one is connected to the variable-range hopping (VRH) charge transfer over localized states of the AB, ρ ($T$) = $AT^m$ exp [($T_0$ / $T$)$^p$] (where $m = p$, $A$ is a constant and $T_0$ is the VRH characteristic temperature) of the Shklovskii-Efros type, or SE ($p$ = 1/2) in # 1, # 3 and of the Mott

type ($p$ = 1/4) in # 2 [6]. This is evident from the analysis of the local activation energy $E_a \equiv d\ ln\ \rho\ /\ d\ (k_B T)^{-1}$ [6] in Fig. 3 (b), which satisfies the equation $\ln [E_a /(k_B T) + m] = \ln p + p \ln T_0 + p \ln (1/T)$ yielding the value of $p$ at a given $m$ as a slope of the plots in Fig. 3 (b).

The SE-VRH conductivity sets in due to microscopic disorder and Coulomb interaction between the charge carriers leading to appearance of the Coulomb gap, Δ, in the spectrum of the density of the localized states (DOS) with width $W$, having the optimal observation when Δ and $W$ are comparable. The Mott-VRH conductivity takes place when the Coulomb interaction between the carriers can be neglected, with condition of $\Delta << W$ being preferable for observation [6].

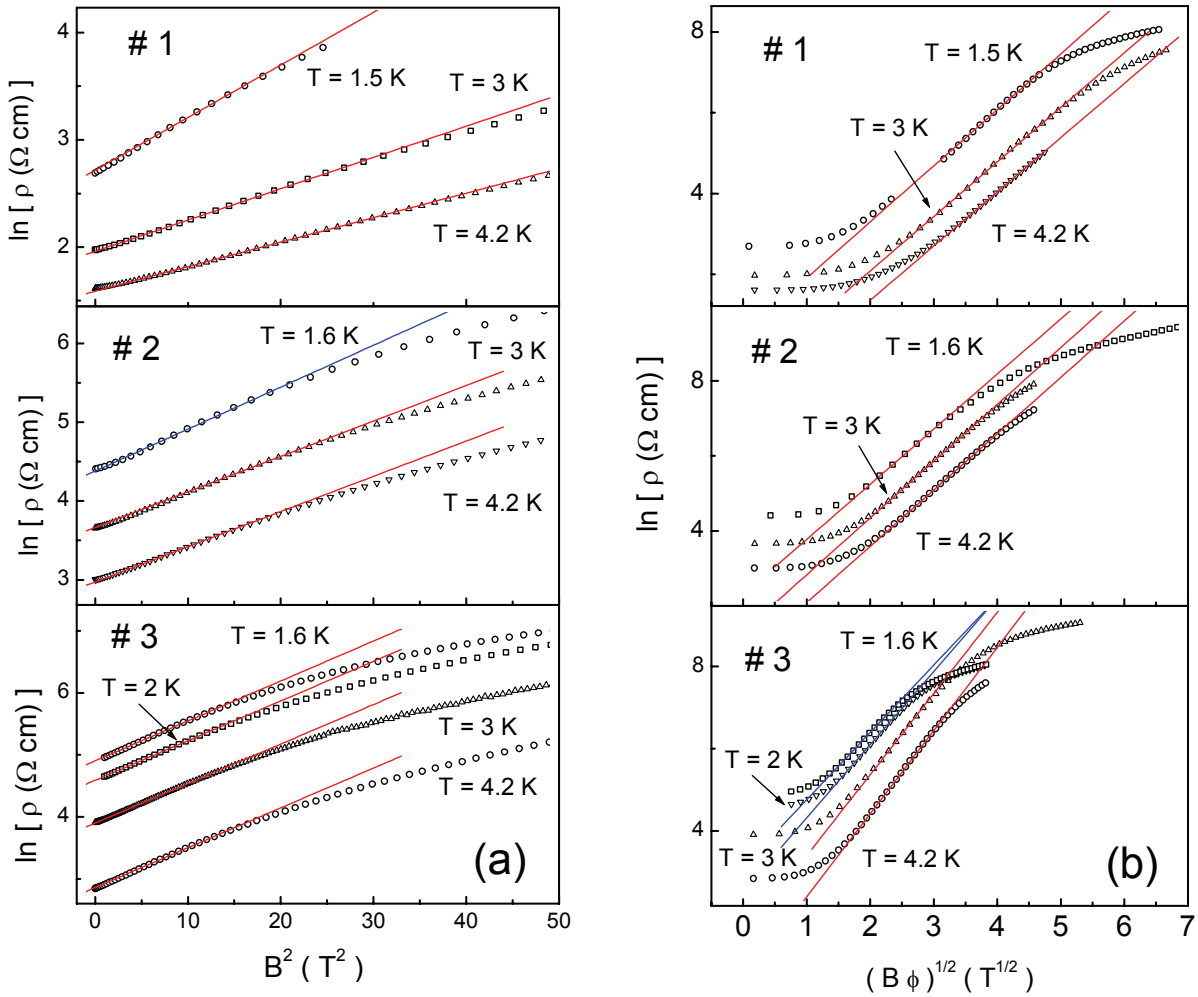


Fig. 4. The dependences of ln ρ on $B^2$ (a) and on $(B\ \varphi)^{1/2}$ (b).

As follows from Fig. 4 (a), the plots of ln ρ vs. $B^2$ below $B \sim 6$ T can be approximated well with linear functions. In # 3 the slope of the plots is constant between 1.6 – 4.2 K. The slope of the corresponding plots for # 2 does not vary between 3 – 4.2 K and increases only slightly between 3 – 1.6 K. In sample # 1 all the plots have different slopes varying with temperature.

In weak fields of $\lambda >> a_0$, where λ is the magnetic length and $a_0$ is the localization radius of charge carriers far from the metal-insulator transition (MIT), positive MR due to shrinkage of the impurity wave functions has been predicted to satisfy the law $\ln \rho_j \sim C_j (T)\ B^2$ for any hopping conductivity mechanism [6] ($j$ = 3, 1, and 2 for # 1, # 2, and # 3, respectively,

reflecting anisotropy of MR in p-CdSb via the anisotropy coefficients $p_j$ [7]). On the other hand, its temperature dependence given by the coefficient $C_j(T)$ is different for each hopping regime: for the nearest - neighbor hopping (NNH) conductivity $C_j$ = const and for the VRH conductivity $C_j(T) \sim T^{-3p}$ [6, 8]. From comparison of the behavior of the slopes of the plots of ln ρ vs. $B^2$ in Fig. 4 (a) with theoretical predictions [6, 8], it follows that contrary to the case of $B = 0$, in # 1 the Mott VRH conductivity takes place between 1.6 – 4.2 K, whereas in # 2 and # 3 the NNH conductivity is observed between 3 – 4.2 and 1.6 – 4.2 K, respectively.

The joint quantitative analysis of the resistivity at $B = 0$ and in weak magnetic fields has yielded a set of microscopic parameters of the charge carriers: Δ, $W$, the localization radius $a$, the density of the localized states (DOS) outside the Coulomb gap $g$, as well as the dielectric permittivity κ, the concentration of acceptors $N_A$, the anisotropy coefficients $p_j$, (see Table I), the critical acceptor concentration for the MIT, $N_C = 6.275\times10^{16}$ cm$^{-3}$, the critical exponents of the localization radius, ν = 1.00, and of the dielectric permittivity, ζ = 1.90, describing the behavior of $a$ and κ near the MIT.

Table I. Values of the microscopic parameters, acceptor concentration, and anisotropy coefficients.

| Sample no. | $N_A$ ($10^{16}$ cm$^{-3}$) | $a$ (Å) | κ | Δ (meV) | $W$ (meV) | $g$ ($10^{16}$ cm$^{-3}$ meV$^{-1}$) | $p_j$ | $p_j^{(cal)}$ | $j$ |
|---|---|---|---|---|---|---|---|---|---|
| 1 | 3.61 | 196 | 127 | 0.30 | 0.50 | 5.94 | 0.839 | 0.839 | 3 |
| 2 | 3.37 | 180 | 108 | 0.18 | 1.28 | 1.31 | 1.008 | 0.897 | 1 |
| 3 | 2.51 | 139 | 66 | 0.49 | 0.91 | 2.16 | 1.182 | 1.327 | 2 |

It can be seen that (i) ν and ζ are close to their theoretical values (1 and 2, respectively) [9], (ii) $N_A$ in all samples is rather close to $N_C$, in agreement with the behavior of the parameters $a$ and κ in Table I (increase with $N_A$), (iii) the anisotropy coefficients $p_j$ are close to calculated values $p_j^{(cal)}$, (iv) Δ is comparable with $W$ in # 1, 3 and $\Delta << W$ in # 2, in agreement with observations of the SE-VRH conductivity in # 1, 3 and the Mott-VRH conductivity in # 2 (Fig. 3 (b)).

In strong fields of $\lambda \le a_0$ the positive MR in the NNH conductivity regime, given by the expression $\ln [\rho(B)]_j \sim \eta_j [B\,\varphi(B)]^{1/2}$ with $\eta_j = q\, p_j^{1/2} [e / (N_A\, a\, \hbar)]^{1/2}$, $q = 0.92$, and $\varphi(B) = a(0) / a(B)$, is determined not only by shrinkage of the impurity wave functions, but also by the dependence of the localization radius on $B$, $a(B)$ [6]. The first reason to $a(B)$ is connected to the dependence of the acceptor activation energy on $B$, given by expressions $E_A(B) = E_A(0)$ for $B << B_0$ and $E_A(B) = E_A \ln^2(B/B_0)$ for $B >> B_0$ [6], $B_0 \equiv \hbar/(ea_0^2)$ being a field where $\lambda = a_0$. In our case of $B_0 = 9.5$ T the interval of high fields corresponds to $B \sim B_0$ or $\lambda \sim a_0$, where $E_A(B)$ cannot be obtained analytically [6]. On the other hand, this function can be approximated well with the relation $E_A(B) = \beta B^{1/3}$, where β is independent of $B$ [6]. The dependence $E_A(B)$ can be found from the plots of $\ln \rho(B, T)$ vs. $T^{-1}$ in the temperature interval of the acceptor freeze-out. Another reason leading to the dependence of $a(B)$ is connected to sensitivity of the MIT to $B$ [10]. Eventually, $\varphi(B) \approx [(3/2)(1+\gamma_0)+(1/6)\gamma_0^2]^* \{(3/2)[1+\gamma_0(B)]+(1/6)\gamma_0^2(B)\}^{-1}\exp\{-\gamma_0[1-\varphi_0(B)]\}$, where $\gamma_0(B) \equiv R_A/a_0(B)$, $\varphi_0(B) = (\beta B^{1/3}/E_A)^{1/2}$ and $R_A = (4\pi N_A/3)^{-1/3}$ is one-half of the mean distance between the acceptors.

As can be seen from Fig. 4 (b), the plots of ln ρ vs. $[B\,\varphi(B)]^{1/2}$ exhibit linear behavior in the interval of $B$ between ~ 4 – 15 T, and their slopes do not depend on temperature at $T \le$ 4.2 K in # 1 and # 2 and between 3 – 4.2 K in # 3, in agreement with the equation for MR above. The values of the slopes $\eta^{(ex)}$ obtained from the plots in Fig. 4 (b), $\eta^{(ex)} = 1.36$, 1.50, and 2.00 T$^{-1/2}$ for # 1, # 2, and # 3, respectively, agree with the calculated values, $\eta_j^{(cal)} =$

1.23, 1.46, and 2.09 $T^{-1/2}$ for # 1, # 2, and # 3, respectively. Hence, the behavior of MR in p-CdSb:Ni in the interval of $B$ between ~ 4 – 15 $T$ is governed by the NNH conductivity, excluding lowest $T$ in # 3, where, however, MR does not agree with any other hopping model for conventional semiconductors requiring increase of the slopes of the plots with decreasing temperature. Deviation of all the plots in Fig. 4 from linearity with increasing $B$ is attributable to the onset of the logarithmic asymptote of $E_A$ ($B$) (see above).

Finally, one can see a general tendency of changing the VRH conductivity, observed at $B = 0$, into the NNH conductivity with increasing magnetic field, which is uncommon in conventional (non-magnetic) semiconductors. However, in p-CdSb:Ni such a tendency is in line with damping of the internal magnetic disorder, connected to presence of magnetic $Ni_{1-x}Sb_x$ nanoclusters by aligning their moments in a field [which takes place already at $B \sim 4$ kG – see Fig. 1 (a)] and reducing the potential barriers between different acceptor sites, which stimulates transitions between nearest neighbors leading to NNH conductivity when $B$ is increased.

### 2.3. Hall effect

The dependence of the Hall resistivity, $\rho_H$, on $B$ shown in Figs. 5 (a) and 5 (b) for one of the investigated samples exhibits a clear non-linearity or strengthening of $\rho_H$ ($B$) with increasing field, being most pronounced below ~ 10 K but still persisting even up to 300 K. The non-linearity of $\rho_H$ ($B$) should be associated with the magnetic subsystem existing in p-CdSb:Ni due to an anomalous contribution to the Hall effect superimposed on the normal one.

In FM compounds $\rho_H = \rho_N + \rho_A$, where $\rho_N = R_0B$, $\rho_A = R_sM$, $R_0$ and $R_s$ are the normal and the anomalous (spontaneous) Hall coefficients, respectively, and $M$ is the magnetization of the material [11]. Applicability of this equation to p-CdSb:Ni, which, strictly speaking, does not belong to FM materials, can be partially substantiated by saturation of the magnetization when $B$ is increased at any $T \leq 300$ K [Fig. 1 (b)], making the second term in Eq. (1) independent of $B$ and tending the plots of $\rho_H$ vs. $B$ to linear functions. As can be seen in Figs. 5 (a) and 5 (b), this takes place in strong magnetic fields, permitting us to obtain $R_0$ and $\rho_A$ as the slope and the interception point of the linear parts with the vertical axis, respectively [11]. The dependences of $R_0$ ($T$) and $\rho_A$ ($T$) are shown in Figs. 5 (c) and 5 (d), respectively.

The Hall concentration, $p_H = 1/(eR_0)$, in the interval of extrinsic conductivity ~ 4.2 – 200 K is determined by the holes activated from the AB to the VB with concentration $p_v$ ($T$), and by the holes in the extended states of the AB, having the fraction $\alpha$, with the concentration $\alpha p_A$ ($T$). This yields the first equation for analysis of the Hall concentration: $p_H$ ($T$) = $p_V$ ($T$) + $\alpha p_A$ ($T$), where $p_A$ ($T$) is the total concentration of the holes in the AB. In addition, from conservation of the holes we have the second equation: $p_A$ ($T$) + $p_V$ ($T$) = $N_A$ (1 – $K$), where $K = N_D / N_A$ is the degree of compensation and $N_D$ is the concentration of compensating donors. Finally, $p_H$ ($T$) is calculated with two equations above, taking into account the non-degeneracy of the holes, and is shown by solid lines in Fig. 6 (a). One can see a good agreement of the calculated curves with the experimental data of $p_H$ ($T$) in the whole interval between 4.2 – 200 K, where the two-band (AB+VB) model above is applicable, at $\alpha = 4\times10^{-3}$, $3.5\times10^{-3}$, and $0.8\times10^{-3}$ for # 1, # 2, and # 3, respectively. The deviations in # 1 taking place below 4.2 K are connected with transition to the hopping conduction, where the model above becomes inapplicable. It can be seen also that calculations with $\alpha = 0$ [the dotted lines in Fig. 6 (a)], deviate from those with $\alpha \neq 0$ only below ~ 10 K. Together with smallness of values of $\alpha$, this means existence of only a quite narrow interval of the extended states in the AB and negligible role of itinerant holes of the AB in the normal Hall effect, excluding only the lowest $T$.

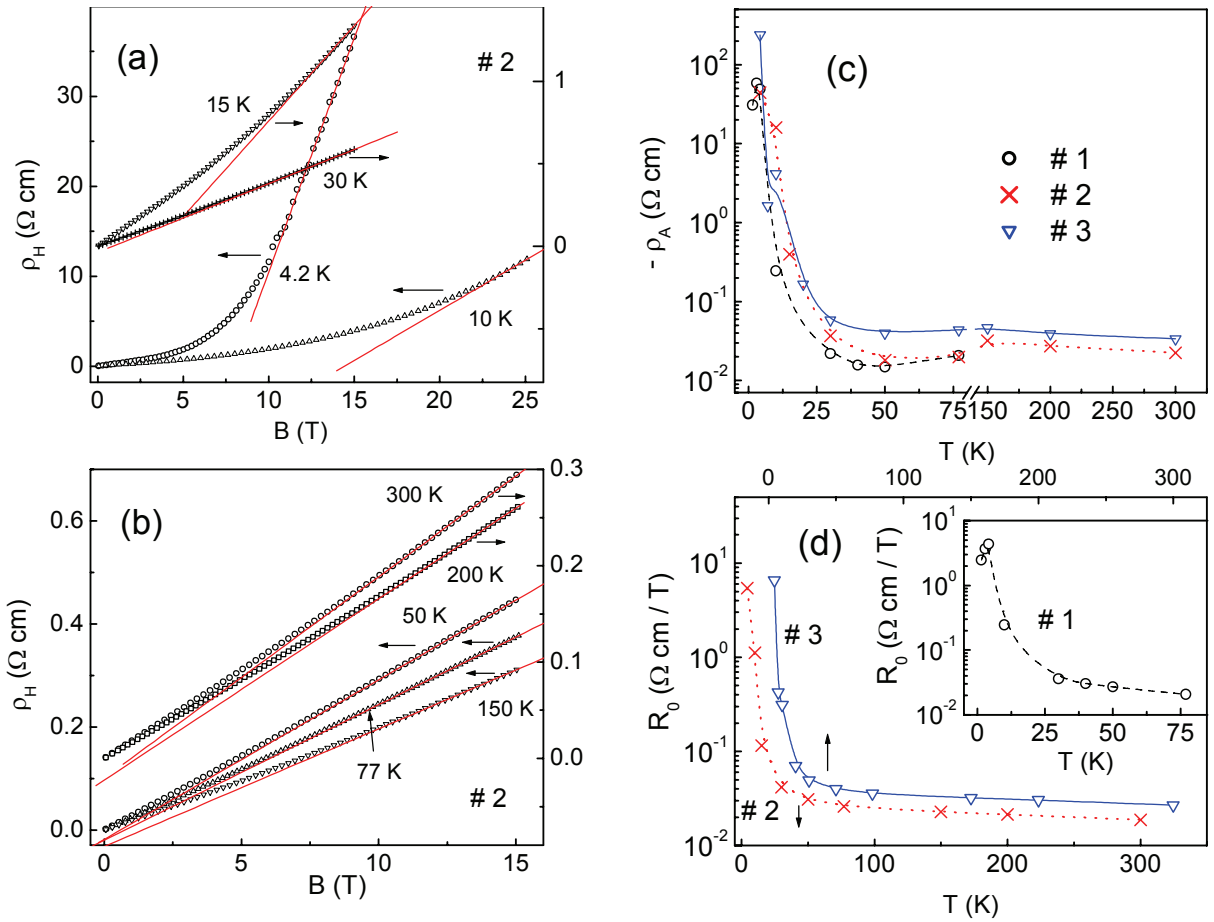


Fig. 5. Plots of $\rho_H$ vs. $B$ for # 2. The lines are linear fits (a, b). Plots of $\rho_A$ vs. $T$ (c) and $R_0$ vs. $T$ (d).

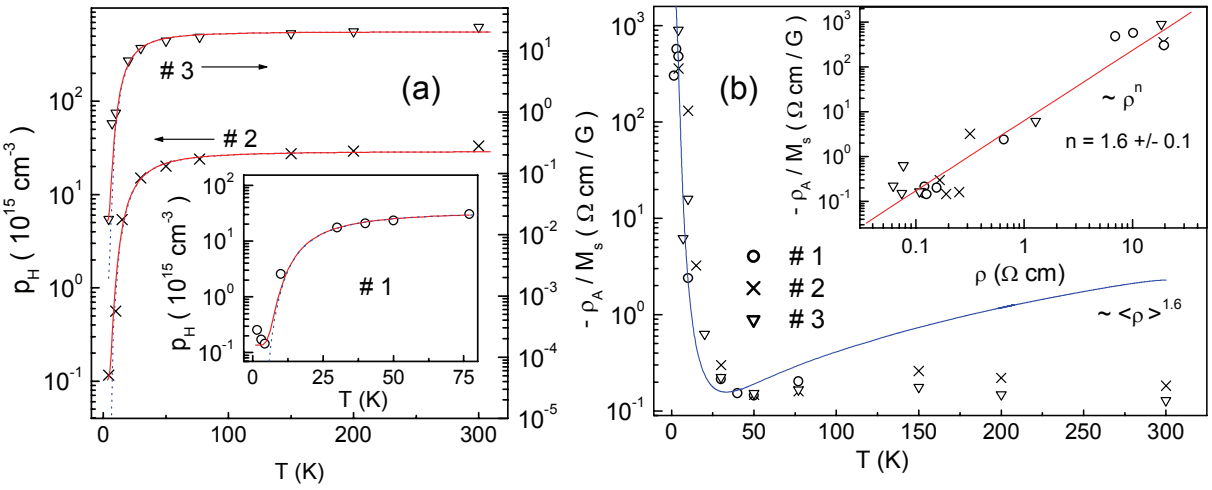


Fig. 6. Plots of $p_H = 1/(eR_0)$ vs. $T$. The lines are calculated as described in the text (a). Plots of - $\rho_A$ / $M_s$ vs. $T$. The line is the low-temperature fit to the experimental data with the function $<\rho(T)>^{1.6}$ (b). Inset to the (b) panel: - $\rho_A$ / $M_s$ vs. ρ in the double-logarithm scale with the line as a linear fit.

As can be seen from Fig. 5 (c), the anomalous contribution to the Hall effect in p-CdSb:Ni is negative, comprising of the weak variation of $\rho_A$ ($T$) above ~ 50 K and a very

strong increase with decreasing $T$ from ~ 50 to 4.2 K. Various microscopic models of the anomalous Hall effect predict the power-law scaling of $\rho_A$ vs. $\rho$, yielding relations like $\rho_A \sim \rho^n$, where $n$ is a constant. To test a possibility of such scaling, we plotted $\rho_A / M_s$ vs. $\rho$ at $T \leq 77$ K [where $M_s$ is the saturation magnetization – see Fig. 1 (b)], in the double-logarithm scale as shown in the inset to Fig. 6 (b). Indeed, these data yield $n = 1.6 \pm 0.1$ within four decades of $\rho_A / M_s$ and more than two decades of $\rho$. In addition, it can be seen that $\rho_A / M_s$ behaves between ~ 1.5 – 77 K similar to the law $<\rho(T)>^{1.6}$, where $<\rho(T)>$ is the mean resistivity obtained by averaging the plots in Fig. 3 (a).

Analysis of the anomalous Hall effect performed in 28 different compounds, belonging to five different types of FM materials, has yielded the value of $n \approx 1.6$ [12], suggesting a broad universality class of this value, although the law $\sigma_A \sim \sigma^n$ (where $\sigma$ and $\sigma_A$ are the conductivity and the anomalous contribution to the Hall conductivity, respectively) has been analyzed [12]. Hence, our value of $n \approx 1.6$ in the resistivity scaling law is likely to reflect this general universality.

## Conclusions

Magnetic properties of the new DMS p-CdSb:Ni give evidence for an assembly of spheroidal Ni-rich $Ni_{1-x}Sb_x$ nanoparticles, which are responsible for magnetic irreversibility and saturation of the magnetization already at the room temperature, and for the magnetic anisotropy. Transformation of the type of the hopping charge transfer from that of the VRH conductivity at $B = 0$ to the NNH conductivity regime in strong magnetic fields, as well as the anomalous contribution to the Hall effect, are also attributable to presence of the $Ni_{1-x}Sb_x$ magnetic nanoclusters in p-CdSb:Ni.

## References


[1] I. Žutić, J. Fabian, and S. Das Sarma, Rev. Mod. Phys., 76, 323, (2004).
[2] R. Laiho, A.V. Lashkul, K.G. Lisunov, E. Lähderanta, I. Ojala, and V.S. Zakhvalinskii, Semicond. Sci. Technol., 21, 228, (2006).
[3] R. Laiho, A.V. Lashkul, E. Lähderanta, K.G. Lisunov, I. Ojala, and V.S. Zakhvalinskii, J. Magn. Magn. Mater., 300, e8, (2006).
[4] E.K. Arushanov, Prog. Crystal Growth Charact., 13, 1, (1986).
[5] L. Sun, Y. Hao, C.L. Chien, and P.C. Searson, IBM J. Res. & Dev., 49, 79, (2005).
[6] B.I. Shklovskii and A.L. Efros, Electronic Properties of Doped Semiconductors, Springer, Berlin, 416, 1984.
[7] R. Laiho, A.V. Lashkul, K.G. Lisunov, E. Lähderanta, M.O. Safonchik, and M.A. Shakhov, J. Phys.: Condens. Matter, 16, 333, (2004).
[8] B.I. Shklovskii, Sov. Phys.-Semicond., 17, 1311, (1983).
[9] T.G. Castner, in: Hopping Transport in Solids, edited by M. Pollak and B. Shklovskii, Elsevier, Amsterdam, Ch. 1, 450, 1991.
[10] N. Mott and E.A. Davies, Electron Processes in Non-Crystalline Materials, Clarendon, Oxford, 368, 1979.
[11] S.V. Vonsovskii, Magnetism, Nauka, Moscow, Ch. 25, 1032, 1971.
[12] T. Fukumura, H. Toyosaki, K. Ueno, M. Nakano, T. Yamasaki, and M. Kawasaki, Jpn. J. Appl. Phys., 46, L642, (2007).